ChemComm

COMMUNICATION

View Article Online
View Journal | View Issue

Cite this: *Chem. Commun.*, 2023, **59**, 3423

Received 14th December 2022,
Accepted 13th February 2023

DOI: 10.1039/d2cc06815j

rsc.li/chemcomm

Stepwise assembly of heterometallic, heteroleptic "triblock Janus-type" metal–organic polyhedra†

Cornelia von Baeckmann,[ab] Sara Ruiz-Relaño,[ab] Inhar Imaz,[ab] Marcel Handke,[ab] Judith Juanhuix,[c] Felipe Gándara,[d] Arnau Carné-Sanchez *[ab] and Daniel Maspoch *[abe]

Increasing the chemical complexity of metal–organic cages (MOCs) or polyhedra (MOPs) demands control over the simultaneous organization of diverse organic linkers and metal ions into discrete caged structures. Herein, we show that a pre-assembled complex of the archetypical cuboctahedral MOP can be used as a template to replicate such caged structure, one having a "triblock Janus-type" configuration that is both heterometallic and heteroleptic.

Discrete metal–organic assemblies featuring empty cavities, generally known as coordination-/metal–organic cages (MOCs)[1,2] or metal–organic polyhedra (MOPs),[3] are receiving great attention due to their rich structural versatility and potential applications in areas such as molecular separation, catalysis, gas storage and biomedical applications.[4–7] To date, most of these assemblies have been constructed from one type of organic linker and one type of metal ion. This is mainly due to the inherent difficulty of controlling the assembly of multiple ions and linkers into such discrete caged structures.[8] However, there is an increasing interest in developing more complex, multicomponent MOCs that may present emerging properties arising from the intra-MOC interactions between different adjacent building blocks, such as increased chemical stability, tandem catalysis, optical or magnetic properties.[9,10] In this context, multicomponent assembly strategies for the construction of cages with two or more metal ions (known as multimetallic cages), or with two or more organic linkers (known as heteroleptic cages), have recently been proposed.[11,12] Specifically, heteroleptic cages have been assembled through the use of shape complementary linkers,[13,14] asymmetric linkers,[15–17] and coordination sphere engineering.[18] Interestingly, heterometallic cages[19] are even rarer than heteroleptic ones. The most common route to them entails the use of heterotopic ligands, which can bind two different metal ions according to their different coordination preferences.[20–22] Alternatively, pre-synthesized hetero-bimetallic clusters can be employed.[23]

Herein, we report a new multicomponent assembly strategy that uses a pre-assembled metal–organic fragment of a known caged structure as a building unit. We envisioned that such a pre-assembled fragment could template the formation of the parent cage when combined with complementary organic linkers and/or metal ions. We reasoned that, if these complementary organic linkers and metal ions were different to those comprising the metal–organic fragment, then our templated synthesis would enable assembly of heteroleptic and bimetallic versions of the parent caged structure. To validate our hypothesis, we applied our strategy to the archetypical cuboctahedral $Cu_{24}bdc_{24}$[24] or $Rh_{24}bdc_{24}$[25] (where bdc stands for 1,3-benzenedicarboxylic acid) MOP, aiming to assemble heteroleptic and/or bimetallic cuboctahedral caged structures having a "triblock Janus-type" configuration.

We began with a retrosynthetic analysis to identify a repetitive, non-interconnected, metal–organic fragment within the cuboctahedral MOP. We found the $Rh_2(bdc)_4$ fragment in the central part (Fig. 1, in magenta) of the cage. It is a Rh(II) paddlewheel complex comprising four bdc linkers, each showing a free carboxylic acid group. We reasoned that four of these pre-synthesized $Rh_2(bdc)_4$ complexes should template the formation of the cuboctahedral MOP when connected *via* 16 additional metal ions and 8 bdc linkers (Fig. 1; in cyan). This assembly involves three different components that ultimately provide access to cuboctahedral MOP whose central portion differs in composition from their two lateral portions, analogously to the well-known, "triblock Janus-type" particles.[26] Accordingly, the cuboctahedral structure of the resulting MOPs will be divided in three distinct parts that exhibit two different chemistries.

[a] *Catalan Institute of Nanoscience and Nanotechnology (ICN2), CSIC, and The Barcelona Institute of Science and Technology, Campus UAB, Bellaterra, Barcelona 08193, Spain. E-mail: arnau.carne@icn2.cat, daniel.maspoch@icn2.cat*
[b] *Departament de Química, Facultat de Ciències Universitat Autònoma de Barcelona, Bellaterra 08193, Spain*
[c] *Alba Synchrotron Light Facility, Cerdanyola del Vallès, Barcelona 08290, Spain*
[d] *Materials Science Institute of Madrid (ICMM), Consejo Superior de Investigaciones Científicas (CSIC), Calle Sor Juana Inés de la Cruz, 3, Madrid 28049, Spain*
[e] *ICREA, Pg. Lluís Companys 23, Barcelona 08010, Spain*

† Electronic supplementary information (ESI) available: Experimental procedures and characterization data. CCDC 2190388, 2190389, 2184149, and 2190390. For ESI and crystallographic data in CIF or other electronic format see DOI: https://doi.org/10.1039/d2cc06815j

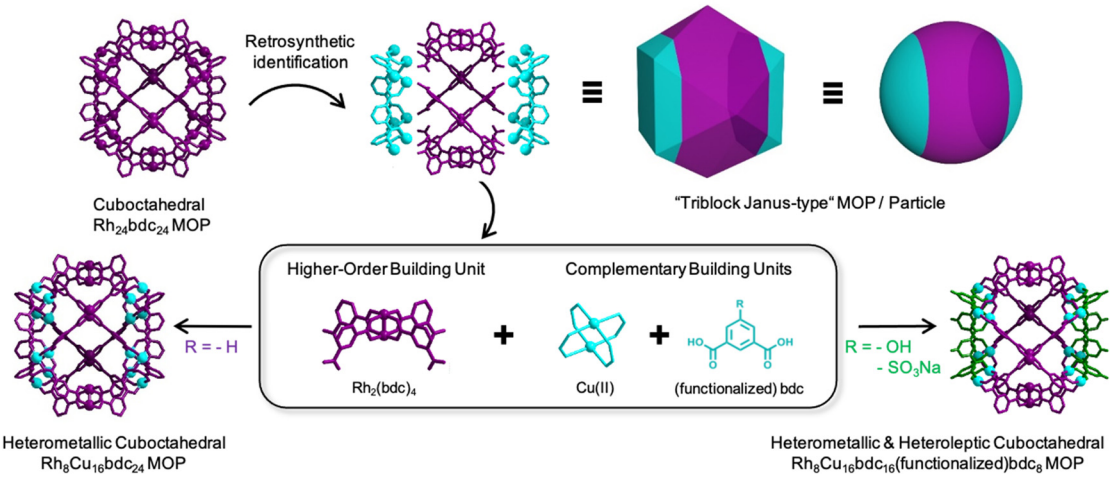

Fig. 1 Schematic illustration of the multicomponent assembly strategy used to synthesize heteroleptic and heterometallic, "triblock Janus-type", MOPs.

Having identified the $Rh_2(bdc)_4$ fragment, we next proceeded with its synthesis. As this complex contains free carboxylic acid groups, we used a protection/deprotection strategy for one of the two carboxylic groups in the bdc linker.[27] In the first step, the carboxylic acid group was protected using 2-(trimethylsilyl)ethanol (see synthetic details in the ESI,† and Fig. S5 and S6). This step was essential, as it prevented reaction of the two carboxylic acid groups of each bdc with Rh(II), thus promoting formation of the protected $Rh_2(bdc)_4$ and consequently, precluding generation of homometallic MOPs or extended structures. The protected $Rh_2(bdc)_4$ complex was synthesized by reacting the half-protected bdc linker with Rh(II) acetate in chlorobenzene at 150 °C overnight. The resulting complex was purified through column chromatography, and its formation was confirmed by nuclear magnetic resonance spectroscopy (NMR) and mass spectrometry (MS) (Fig. S7 and S8, ESI†). Finally, the four carboxylic acid groups of the complex were deprotected by treatment with tetra-*n*-butylammonium fluoride at room temperature overnight. The formation of $Rh_2(bdc)_4$ with the four deprotected carboxylic acid groups was confirmed by single-crystal X-ray diffraction (SCXRD, Fig. 2a), ^{1}H NMR and MS (Fig. S9–S11, ESI†).

With the complex in hand, we first used it as a building block to assemble a three-component, bimetallic cuboctahedral MOP. Based on the expected stoichiometry between the three components in the final caged structure, $Rh_2(bdc)_4$ was reacted with 4 mol. eq. of $Cu(NO_3)_2$ and 2 mol. eq. of bdc in dimethylacetamide (DMA) at room temperature for 1 week to obtain a green solid, herein named HET-MOP-1 (where HET stands for heteroleptic and/or heterometallic). The solid was washed with DMA and diethyl ether to remove unreacted reagents and left to dry in open air (yield: 13%). To confirm the MOP structure, we performed N_2 and CO_2 adsorption of the obtained solid (Fig. S12, ESI†), observing a Brunauer–Emmett–Teller (BET) surface area of 411 $m^2\ g^{-1}$ and a maximum uptake at 1 bar and 298 K of 1.03 mmol $CO_2\ g^{-1}$. Importantly, the solid could be redissolved in dimethylformamide (DMF), which suggested that the product of the reaction is not an extended framework

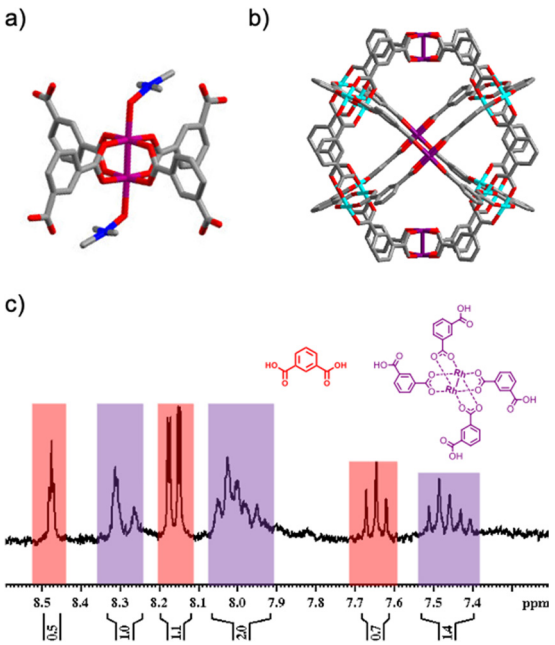

Fig. 2 (a and b) Crystal structures of (a) deprotected $Rh_2(bdc)_4$ complex and (b) HET-MOP-1. (c) ^{1}H NMR spectrum (300 MHz, DMSO-d_6) indicating disassembly of the structure into the $Rh_2(bdc)_4$ complex (purple) and the free bdc linker (red).

but a discrete molecule. Exposure of the DMF solution in the presence of 4-*tert*-butylpyridine to ether vapors let to formation of crystals suitable for SCXRD, which revealed formation of the targeted, bimetallic, cuboctahedral HET-MOP-1, of formula $[Rh_8Cu_{16}(bdc)_{24}]$ (Fig. 2b). However, in this structure, the position of each metal could not be elucidated, due to the high symmetry of the cage, whereby Rh(II) and Cu(II) can occupy the same crystallographic positions (Fig. S13, ESI†), and where all paddlewheels are topologically equivalent, corresponding to the only kind of vertex present in the cuboctahedron.[28,29] Considering this, a satisfactory refinement was obtained when the occupancy of each metal site was fixed to 1/3 for Rh(II) and 2/3

for Cu(II), as expected from the molecular formula of HET-MOP-1. Note that the powder-XRD pattern matched the calculated pattern, confirming the purity of the sample (Fig. S14, ESI†).

Next, we further confirmed the bimetallic character of the cuboctahedral HET-MOP-1 by matrix-assisted laser desorption/ionization-time-of-flight (MALDI-TOF) spectrometry, from which the solubilized HET-MOP-1 showed a peak at m/z = 5779.8, which is in very good agreement with the expected molecular mass ([M + H$^+$] = 5779.4) (Fig. S15, ESI†). Also, high resolution SEM/EDX performed on several single crystals confirmed the presence of both Rh and Cu in the expected proportion of 1 : 2 (Rh/Cu) (Fig. S16, ESI†). Furthermore, EDX mapping performed on several single crystals of HET-MOP-1 revealed the homogeneous distribution of both metal ions through the crystal (Fig. S17, ESI†). In addition, UV-Vis analysis of the DMF solution of HET-MOP-1 revealed the presence of two broad bands centered at 588 nm and 746 nm, which were ascribed to the λ_{max} of both Rh(II)- and Cu(II)-based paddlewheels, respectively (Fig. S18, ESI†).[30,31] Finally, to further demonstrate the integrity of $Rh_2(bdc)_4$ throughout the self-assembly process, HET-MOP-1 was disassembled into its initial components by exposing it to mild acidic conditions at room temperature. The titration of a DMF solution of HET-MOP-1 with HCl was monitored through UV-Vis (Fig. S19, ESI†). Among the two types of paddlewheels forming HET-MOP-1, titration revealed that the Cu(II) one could be fully disassembled, whereas the Rh(II) paddlewheel could not be, as it was maintained even upon addition of 12 mol. eq. of acid. This disassembly experiment further confirms the absence of metal exchange between the $Rh_2(bdc)_4$ and Cu(II) ions during the synthesis of the HET-MOP-1, which is ascribed to inertness of the equatorial position of Rh(II)-carboxylate paddlewheel structures.[10] The ^{1}H-NMR spectrum of the acid-treated HET-MOP-1 (in DMSO-d_6) further confirmed selective disassembly of the MOP into the deprotected $Rh_2(bdc)_4$ complex and bdc linkers at a molar ratio of 1 : 2, as expected from the molecular formula of HET-MOP-1 (Fig. 2c and Fig. S20 and S21, ESI†).

We then envisioned incorporating a functionalized bdc linker into the self-assembly process to assemble cuboctahedral MOPs that would be both bimetallic and heteroleptic. With the use of functionalized bdc linkers, we expected to introduce such functional groups into both side portions of the "triblock Janus-type" MOPs. We imagined replacing the complementary bdc with functionalized versions of it, at its 5-position (Fig. 3a). Thus, we decided to run a co-assembly reaction of Cu(II), $Rh_2(bdc)_4$ and either 5-hydroxyl-isophthalic acid (OH-bdc) or 5-sulfoisophthalic acid sodium salt ($NaSO_3$-bdc). In a first assembly, OH-bdc, $Cu(NO_3)_2$ and $Rh_2(bdc)_4$ were reacted in DMA at room temperature for 24 hours, after which a green precipitate (hereafter named HET-MOP-2) was obtained, which was isolated and washed with DMA and ether (yield: 14%). The green solid was solubilized in DMF and exposed to ether vapours to obtain crystals suitable for SCXRD. Next, a second assembly reaction was performed under similar conditions with respect to the stoichiometry of the different building blocks (85 °C for 48 hours), except that $NaSO_3$-bdc was used instead of OH-bdc. This led to a similar product, named HET-MOP-3 (yield: 25%). Here, single crystals suitable for SCXRD analysis were directly harvested from the solvothermal reaction.

SCXRD confirmed formation of two cuboctahedral cages built up from two types of linkers (bdc and either OH-bdc or $NaSO_3$-bdc) and two types of metal ions [Cu(II) and Rh(II)] (Fig. 3b and e). Analysis of the crystal structures of HET-MOP-2 and HET-MOP-3, which followed the same principles as for HET-MOP-1, confirmed occupancy values at each metal site of 1/3 for Rh(II) and of 2/3 for Cu(II). Similarly, based on these symmetric effects, the electron density of all functional groups

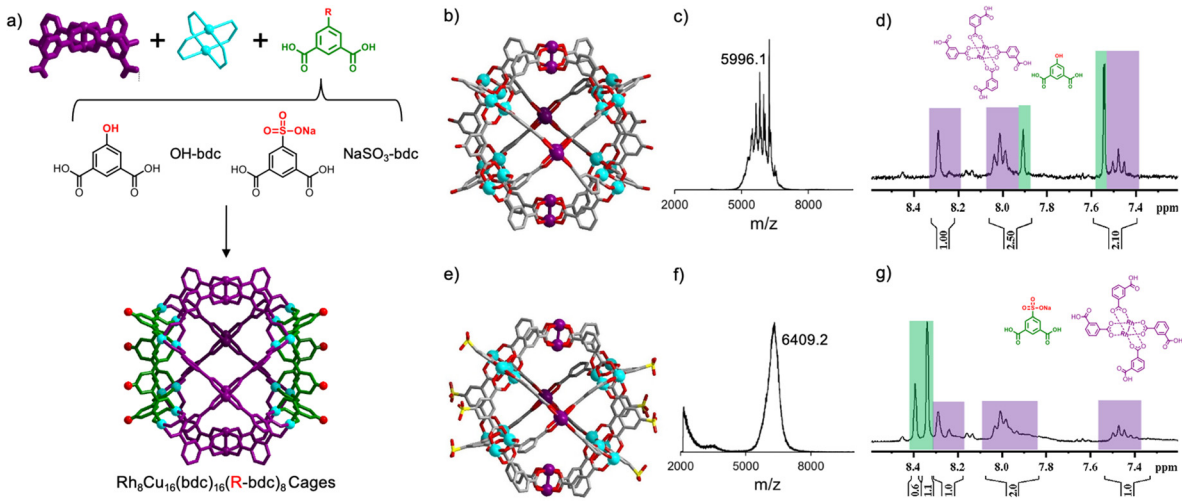

Fig. 3 (a) Schematic illustration of the formation of HET-MOP-2 and HET-MOP-3. (b) Crystal structure of HET-MOP-2. (c) MALDI-TOF spectrum of HET-MOP-2, with the peak at m/z = 5996.1 highlighted. (d) ^{1}H NMR spectrum (300 MHz, DMSO-d_6) confirming the disassembly of HET-MOP-2 into its constituent $Rh_2(bdc)_4$ complex (purple) and OH-bdc linker (green). (e) Crystal structure of HET-MOP-3. (f) MALDI-TOF spectrum of HET-MOP-3, with the peak at m/z = 6409.2 highlighted. (g) ^{1}H NMR spectrum (300 MHz, DMSO-d_6) confirming the disassembly of HET-MOP-3 into its constituent $Rh_2(bdc)_4$ complex (purple) and $NaSO_3$-bdc linker (green).

of the linkers are a sum of hydrogen (for bdc) and OH (for OH-bdc) or $NaSO_3$ (for $NaSO_3$-bdc). Here, the molecular formula suggested a ratio of 1/3 R-bdc (R = OH, $NaSO_3$) to 2/3 bdc, which were confirmed during the refinement process. Powder-XRD patterns further confirmed the purity of the samples (Fig. S22 and S28, ESI†). We then sought further evidence of formation of the above heterometallic and heteroleptic cages, through MALDI-TOF (Fig. 3c and f), which revealed a peak at m/z = 5996.6 (for HET-MOP-2) and m/z = 6409.2 (for HET-MOP-3), which are in agreement with the corresponding postulated formulas: $[Rh_8Cu_{16}(bdc)_{16}(OH\text{-}bdc)_8]$ ($[M + H_3O^+ + DMF]$ = 5996.3); and $[Rh_8Cu_{16}(bdc)_{16}(NaSO_3\text{-}bdc)_8]$ ($[M + H^+]$ = 6409.6). Consistently, mild acidic disassembly of both HET-MOP-2 and HET-MOP-3 at room temperature revealed the expected molar ratio of 1 : 2 ($Rh_2(bdc)_4$ complex/R-bdc) (Fig. 3d and g) (for UV/Vis analysis see Fig. S23 and S29, ESI†). Identification of $Rh_2(bdc)_4$ in this disassembly process clearly evidenced preservation of this complex throughout the self-assembly process, thus excluding any possible ligand exchange. Acidic disassembly at high temperature (T = 100 °C) enabled full disassembly of both HET-MOP-2 and HET-MOP-3 into their corresponding free linkers (Fig. S24 and S30, ESI†). ^{1}H-NMR spectra of the resulting solutions revealed molar ratios of 1 : 0.5 for HET-MOP-2 (bdc/OH-bdc) and HET-MOP-3(bdc/$NaSO_3$-bdc), which are in good agreement with the expected values (1 : 0.5). High-resolution SEM/EDX analysis and EDX mapping of single crystals confirmed the expected Cu : Rh ratio (2/3 Cu and 1/3 Rh) and the homogeneous distribution of both metals within the same crystal for both HET-MOP-2 and HET-MOP-3 (Fig. S25, S26, S31 and S32, ESI†). Finally, we found that HET-MOP-2 is porous to N_2 (BET surface area = 359 $m^2\ g^{-1}$) and CO_2 (uptake at 1 bar and 298 K = 1.2 mmol $CO_2\ g^{-1}$), whereas HET-MOP-3 is only porous to CO_2 (uptake at 1 bar and 298 K = 1.2 mmol $CO_2\ g^{-1}$; Fig. S27 and S33, ESI†).

In conclusion, we have developed a stepwise synthetic method that employs pre-assembled complexes of a known cage to replicate it with a multicomponent character. The value of our method stems from the fact that the pre-assembled $Rh_2(bdc)_4$ complex determines the position of both the additional inorganic and organic building blocks in the final cuboctahedral structure. This enables convergence of four different molecules (two types of metal ions + two types of organic linkers) into a single, well-defined caged structure. We are confident that this degree of structural control in discrete metal–organic assemblies should pave the way to achieving greater chemical complexity in cages, expanding the catalog of synthetically accessible cages, and optimizing cages for functional applications such as catalysis and gas storage.

This work was supported by the Spanish MINECO (project RTI2018-095622-B-I00), the Catalan AGAUR (project 2021 SGR 00458), the CERCA Program/Generalitat de Catalunya, and the MCIN/AEI/10.13039/501100011033. ICN2 is supported by the Severo Ochoa program from the Spanish MINECO (grant SEV-2017-0706). The project that gave rise to these results received the support of a fellowship (LCF/BQ/PR20/11770011) from "la Caixa" Foundation (ID 100010434). C.v.B. thanks the Austrian Science Fund (FWF), Erwin Schrödinger fellowship for supporting the project J 4637.

Conflicts of interest

There are no conflicts to declare.

Notes and references

1 S. Zarra, D. M. Wood, D. A. Roberts and J. R. Nitschke, *Chem. Soc. Rev.*, 2015, **44**, 419–432.
2 M. Yoshizawa, J. K. Klostermann and M. Fujita, *Angew. Chem., Int. Ed.*, 2009, **48**, 3418–3438.
3 D. J. Tranchemontagne, Z. Ni, M. O'Keeffe and O. M. Yaghi, *Angew. Chem., Int. Ed.*, 2008, **47**, 5136–5147.
4 D. Zhang, T. K. Ronson, Y.-Q. Zou and J. R. Nitschke, *Nat. Rev. Chem.*, 2021, **5**, 168–182.
5 A. J. Gosselin, C. A. Rowland and E. D. Bloch, *Chem. Rev.*, 2020, **120**, 8987–9014.
6 S. K. Samanta and L. Isaacs, *Coord. Chem. Rev.*, 2020, **410**, 213181.
7 B. S. Pilgrim and N. R. Champness, *ChemPlusChem*, 2020, **85**, 1842–1856.
8 T. Tateishi, M. Yoshimura, S. Tokuda, F. Matsuda, D. Fujita and S. Furukawa, *Coord. Chem. Rev.*, 2022, **467**, 214612.
9 D. Nam, J. Kim, E. Hwang, J. Nam, H. Jeong, T.-H. Kwon and W. Choe, *Matter*, 2021, **4**, 2460–2473.
10 A. Khobotov-Bakishev, C. von Baeckmann, B. Ortín-Rubio, L. Hernández-López, A. Cortés-Martínez, J. Martínez-Esaín, F. Gándara, J. Juanhuix, A. E. Platero-Prats, J. Faraudo, A. Carné-Sánchez and D. Maspoch, *J. Am. Chem. Soc.*, 2022, **144**, 15745–15753.
11 H. Li, Z.-J. Yao, D. Liu and G.-X. Jin, *Coord. Chem. Rev.*, 2015, **293**, 139–157.
12 S. Pullen and G. H. Clever, *Acc. Chem. Res.*, 2018, **51**, 3052–3064.
13 K. Wu, D. Zhang, C. Drechsler, J. J. Holstein and G. H. Clever, *Angew. Chem., Int. Ed.*, 2021, **60**, 6403–6407.
14 S. Saha, I. Regeni and G. H. Clever, *Coord. Chem. Rev.*, 2018, **374**, 1–14.
15 S. Pullen, J. Tessarolo and G. H. Clever, *Chem. Sci.*, 2021, **12**, 7269–7293.
16 S. C. Bete and M. Otte, *Angew. Chem., Int. Ed.*, 2021, **60**, 18582–18586.
17 W. M. Bloch and G. H. Clever, *Chem. Commun.*, 2017, **53**, 8506–8516.
18 B. Chen, J. J. Holstein, A. Platzek, L. Schneider, K. Wu and G. H. Clever, *Chem. Sci.*, 2022, **13**, 1829–1834.
19 L. S. Lisboa, D. Preston, C. J. McAdam, L. J. Wright, C. G. Hartinger and J. D. Crowley, *Angew. Chem., Int. Ed.*, 2022, **61**, e202201700.
20 Y.-Y. Zhang, W.-X. Gao, L. Lin and G.-X. Jin, *Coord. Chem. Rev.*, 2017, **344**, 323–344.
21 J.-F. Ayme, J. E. Beves, C. J. Campbell and D. A. Leigh, *Angew. Chem., Int. Ed.*, 2014, **53**, 7823–7827.
22 J. P. Carpenter, T. K. Ronson, F. J. Rizzuto, T. Héliot, P. Grice and J. R. Nitschke, *J. Am. Chem. Soc.*, 2022, **144**, 8467–8473.
23 J. M. Teo, C. J. Coghlan, J. D. Evans, E. Tsivion, M. Head-Gordon, C. J. Sumby and C. J. Doonan, *Chem. Commun.*, 2016, **52**, 276–279.
24 M. Eddaoudi, J. Kim, J. B. Wachter, H. K. Chae, M. O'Keeffe and O. M. Yaghi, *J. Am. Chem. Soc.*, 2001, **123**, 4368–4369.
25 S. Furukawa, N. Horike, M. Kondo, Y. Hijikata, A. Carné-Sánchez, P. Larpent, N. Louvain, S. Diring, H. Sato, R. Matsuda, R. Kawano and S. Kitagawa, *Inorg. Chem.*, 2016, **55**, 10843–10846.
26 A. H. Gröschel, A. Walther, T. I. Löbling, J. Schmelz, A. Hanisch, H. Schmalz and A. H. E. Müller, *J. Am. Chem. Soc.*, 2012, **134**, 13850–13860.
27 S. Matasunaga, K. Hasada, K. Sugiura, N. Kitamura, Y. Kudo, N. Endo and W. Mori, *Bull. Chem. Soc. Jpn.*, 2012, **85**, 433–438.
28 D. J. Tranchemontagne, Z. Ni, M. O'Keeffe and O. M. Yaghi, *Angew. Chem., Int. Ed.*, 2008, **47**, 5136–5147.
29 M. O'Keeffe, M. A. Peskov, S. J. Ramsden and O. M. Yaghi, *Acc. Chem. Res.*, 2008, **41**, 1782–1789.
30 P. Mosae Selvakumar, S. Nadella, J. Sahoo, E. Suresh and P. S. Subramanian, *J. Coord. Chem.*, 2013, **66**, 287–299.
31 A. Carné-Sanchez, J. Albalad, T. Grancha, I. Imaz, J. Juanhuix, P. Larpent, S. Furukawa and D. Maspoch, *J. Am. Chem. Soc.*, 2019, **141**, 4094–4102.

